Phase behavior of colloidal silica rods

Anke Kuijk,[a] Dmytro V. Byelov,[b] Andrei V. Petukhov,[b] Alfons van Blaaderen[a] and Arnout Imhof[a]

Received 26th April 2012, Accepted 6th June 2012
DOI: 10.1039/c2fd20084h

Recently, a novel colloidal hard-rod-like model system was developed which consists of silica rods [Kuijk *et al.*, *JACS*, 2011, **133**, 2346]. Here, we present a study of the phase behavior of these rods, for aspect ratios ranging from 3.7 to 8.0. By combining real-space confocal laser scanning microscopy with small angle X-ray scattering, a phase diagram depending on concentration and aspect ratio was constructed, which shows good qualitative agreement with the simulation results for the hard spherocylinder system. Besides the expected nematic and smectic liquid crystalline phases for the higher aspect ratios, we found a smectic-*B* phase at high densities for all systems. Additionally, real-space measurements on the single-particle level provided preliminary information on (liquid) crystal nucleation, defects and dynamics in the smectic phase.

1 Introduction

The phase behavior of anisotropic particles is richer than that of spherical particles. In addition to the gas, liquid, crystal and glass phases that were observed for spheres, anisotropic particles such as rods can form liquid crystal phases: additional phases between the liquid and crystal phase that possess long-range orientational and positional order in less than the three dimensions of a 3D crystal. One of the first theoretical explanations for the formation of a nematic liquid crystal phase was provided by Onsager in 1949.[1] He explained why the transition from the isotropic to the nematic phase for long, hard rods could be purely entropy based. Later, computer simulations showed that not only nematic, but also smectic and crystalline phases can occur in systems of hard spherocylinders (HSC).[2,3] The formation of liquid crystal phases depends on the concentration and aspect ratio of the rodlike particles. Also, the shape of the particles is an important parameter. Ellipsoids, for example, only show a nematic liquid crystal phase, while for spherocylinders a nematic and a smectic phase were found.[4]

The experimental verification of the simulation results requires a system of hard rods. The majority of experimental systems that have been used to study liquid crystalline phases only allows for measurements on the many-particle level, either because of their small dimensions or due to their high refractive index. Therefore, research on rod-like particles has been limited to the many-particle level and reciprocal space for a long time. Even though it is possible to distinguish smectic phases of, for instance, *fd*-virus using light microscopy, the individual particles can only be imaged this way when a doped system is used (in which 1 on every 30 000 particles is labeled).[5,6] Imaging all individual particles is not possible in this system using light

[a]*Soft Condensed Matter, Debye Institute for Nanomaterials Science, Department of Physics, Utrecht University, Princetonplein 5, 3584 CC Utrecht, The Netherlands. E-mail: A.Imhof@uu.nl*
[b]*Van 't Hoff Laboratory for Physical and Colloid Chemistry, Debye Institute for Nanomaterials Science, Department of Chemistry, Utrecht University, Padualaan 8, 3584 CH Utrecht, The Netherlands*

microscopy. Studies involving mineral liquid crystals, like boehmite or goethite are also based on many-particle effects such as birefringence and scattering.[7–10] The first real-space data on 3D systems of rods on the single-particle level were reported by Maeda *et al.* in 2003.[11] They showed the process of self-ordering for several aspect ratios of inorganic rods. Although their observations already provided a lot of information that is hard or impossible to obtain from scattering experiments, the amount of information was limited by the systems that were used. The systems that were studied by Maeda consisted of rods with high refractive indices. The resulting strong scattering makes it hard to obtain 3D data for these systems.

Systems of anisotropic model colloids that do allow for 3D data acquisition, because their refractive index can be matched to that of the solvent, include PMMA ellipsoids,[12,13] silica dumbbells[14] and silica rods produced either by strong anisotropic etching of structured silicon wafers[15] or by our recently developed 'bulk' synthesis method.[16] Of these systems, the system of 'bulk' silica rods is the only one that has aspect ratios high enough to form liquid crystal phases, a shape that allows for both nematics and smectics to form and that can be produced in sufficient quantity to perform phase separation experiments. Furthermore, research has shown that silica colloids are a good model system for the hard sphere system if they are always present and attractive van der Waals interactions can be sufficiently suppressed.[17,18] Therefore, we expect the system of silica rods to be a good model system for the hard rod system as well. However, there are some differences between our experimental rods and a perfect HSC-system. Firstly, the rods are initially bullet-shaped. Nevertheless, they resemble the shape of a spherocylinder (a cylinder capped with a hemisphere on both ends) more and more after coating with several extra layers of silica, including fluorescent labeling, to make them suitable for confocal laser scanning microscopy (CLSM).[18,19] Secondly, experimental colloidal systems always have an inherent polydispersity which influences their phase behavior. For HSC-systems it was shown that a smectic phase can only form if the length polydispersity is below 18%.[20] Since the polydispersity of the silica rods is around 10%, the system is expected to be able to form smectic phases. Thirdly, our colloidal dispersion of silica rods is a charge-stabilized system. It is known that charges increase the effective diameter of needles,[21] and also that colloidal charges and weak-screening conditions lead to a decreased aspect ratio of charged rods.[22] For equivalent systems of charged spheres, it was shown that the effective increased diameter due to charge can be used to map results on phase behavior on the hard sphere model.[23,24] However, since theoretical studies showed that charge tends to stabilize the positionally ordered phases, especially the columnar phase, and decrease the nematic and smectic phase,[25,26] it is not obvious that the same strategy can be followed for rod-systems unless the Debye screening length is very small as compared to the smallest particle dimension.

In this paper, we describe the phases found in sediments of rods using small angle X-ray scattering (SAXS) and real space CLSM measurements. By combining the results of both methods a phase diagram was constructed depending on aspect ratio and volume fraction. Furthermore, we show real-space measurements on the single-particle level that provide detailed information on (liquid) crystal nucleation, defects and dynamics in concentrated phases.

2 Experimental

2.1 Dispersions

The properties of the systems used for the SAXS and CLSM measurements are summarized in Table 1. All silica rods, which are shown in Fig. 1, were prepared as described by Kuijk *et al.*[16,19] Systems B31 and B35 consist of a non-fluorescent core, a 30 nm fluorescein isothiocyanate (FITC) labeled inner shell and a 190 nm non-fluorescent outer shell. The rods of B36 were not coated after synthesis. Systems

Table 1 Properties of the systems of colloidal silica rods that were used in this work. Here, L is the length of the rods, D the diameter, σ the polydispersity, φ the volume fraction and l_g the gravitational height

	L/μm	σ_L/%	D/nm	σ_D/%	L/D	φ	l_g/μm
B31	2.37	10	640	7.5	3.7	0.10	0.7
B35	3.3	10	550	11	6.0	0.10	0.7
B36	1.9	15	235	17	8.0	0.128	6.5
B48	2.6	8.5	630	6.3	4.1	0.10	0.7
N51	2.66	10	530	6.3	5.0	0.105	0.9

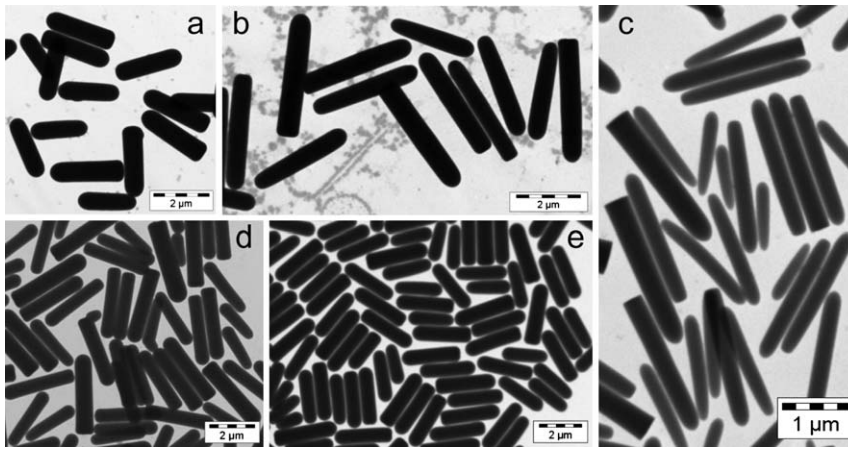

Fig. 1 TEM images of the systems of silica rods used. (a) B31. (b) B35. (c) B36. (d) N51. (e) B48. The dimensions of the rods are listed in Table 1.

B48 and N51 consist of a rhodamine isothiocyanate (RITC) labeled core and a 175 or 150 nm non-fluorescent shell, respectively.

Rods with $L = 1.9$ μm and $D = 420$ nm were used in the optical Bragg-reflection measurements. A 6 cm high capillary was filled with an initial volume fraction of 0.2 and afterwards left to sediment.

For the diffusion measurements in the smectic phase, a system of rods with length $L = 1.4$ μm, diameter $D = 280$ nm and polydispersities of $\sigma_L = 6\%$ and $\sigma_D = 10\%$ was used. This system was coated with a 20 nm FITC-labeled layer only. For single particle observation, a system of FITC labeled rods of $L = 2.2$ μm, $D = 340$ nm, $\sigma_L = 10\%$ and $\sigma_D = 15\%$ was mixed with a system of unlabeled rods of $L = 2.1$ μm, $D = 250$ nm, $\sigma_L = 9\%$ and $\sigma_D = 17\%$. The ratio of labeled to unlabeled particles was 1 : 100.

Particle size distributions were determined by transmission electron microscopy (TEM), using a Technai 10 or 12 electron microscope (FEI company). The average length $\langle L \rangle$ and diameter $\langle D \rangle$ of the rods, as well as their standard deviation δ, were measured using iTEM imaging software. The polydispersity is defined as $\sigma_L = \delta_L / \langle L \rangle$. For each sample 50 to 100 particles were measured.

The solvent mixture of all systems consisted of dimethylsulfoxide (DMSO, ≥99.9%, Sigma-Aldrich) and ultrapure water (Millipore system). The particles were dispersed in DMSO first, after which water was added until the refractive index was matched by eye. This resulted in a 10/0.85 volume ratio of DMSO/water ($n = 1.47$).

2.2 Confocal microscopy

Confocal microscopy measurements were performed with a Leica SP2 or a Nikon C1 confocal, of which the Nikon was used to study samples that were positioned in a vertical position (gravity along the length of the capillary) using a 90° tilted Leica TCS NT inverse microscope frame. A 63× oil immersion objective with a numerical apperture of 1.4 was used (Leica PLAN APO). The dispersions were studied in capillaries of 1 or 2 mm wide and 0.1 mm high with glass walls of about 100 μm thick (Vitrotubes). The capillaries were sealed with candle wax first and two-component epoxy glue (Bison Kombi rapide) on top of that.

The coordinates of the rods in confocal microscopy images in which the rods were oriented perpendicular to the plane of view (so that they look like spheres in the image, see for instance Fig. 8) were obtained by a method similar to that of Crocker and Grier.[27]

2.3 X-Ray experiments

Small angle X-ray scattering (SAXS) measurements were performed at the DUBBLE beamline of the European Synchrotron Radiation Facility (ESRF, Grenoble, France). Flat glass capillaries (Vitrocom) with internal dimensions of $0.1 \times 1 \times 100$ mm^3 were filled with several dispersions of rods (see Table 1). The glass thickness of these capillaries is about 100 μm. The capillaries were closed by melting the ends and covering them with two-component epoxy glue (Bison Kombi rapide) to ensure full closure. After filling, the capillaries were kept in a vertical position to allow the establishment of a sedimentation equilibrium profile. The samples were prepared in a period of three weeks before measuring. For these measurements the microradian resolution setup was used.[28] Here, a CCD detector (Photonic Science Ltd) with pixel size 9×9 μm was placed at a distance of 7.4 m from the sample. The selected wavelength of the X-rays was 0.095 nm, the beam size at the sample position about 0.3 mm. The intensity profiles shown in Fig. 4 were further calculated by integrating over a circular sector containing the area of interest in the scattering patterns.

3 Results and discussion

The phase behavior of colloids depends strongly on the volume fraction of the dispersion. Since a system of silica rods in DMSO/water was used, the volume fraction in our experiments was not constant, but changed during sedimentation. When the sedimenting system had reached an equilibrium, the balance between the gravitational pressure and the osmotic pressure caused a gradient in volume fraction depending on the height in the sample. As a consequence, a range of volume fractions, and therefore multiple phases, could be studied in one sediment.[29]

The formation of a sediment is displayed in Fig. 2, which shows photographs of a typical sample after several sedimentation times. The dark area at the bottom was caused by a drop of glue, which covered the lowest 5 mm of the capillary and deflected the light from the white-light source that illuminated the sediment from behind. From Fig. 2 we calculated the sedimentation velocity v_{sed} by measuring the position of the interface (indicated by the upper line) in time. Based on a model for the sedimentation of cylinders,[30,31] a theoretical v_{sed} of 6.5 μm min^{-1} was calculated in the dilute limit for hard rods. Experimentally, we measured a much lower and decreasing v_{sed} of 0.20 μm min^{-1} for days 11 to 14, to 0.17 μm min^{-1} for the next two days and 0.06 μm min^{-1} for days 16 to 18. The lower experimentally measured v_{sed} as well as its decrease in time are caused by the increasing volume fraction in the sediment.[32]

The second line from above in Fig. 2 denotes the interface between a region that shows Bragg reflections (layered phase) and a region that does not (isotropic or nematic phase). Bragg reflections occur when there is periodicity in the sample, so they are an indication of order. The first Bragg reflections were observed after 5

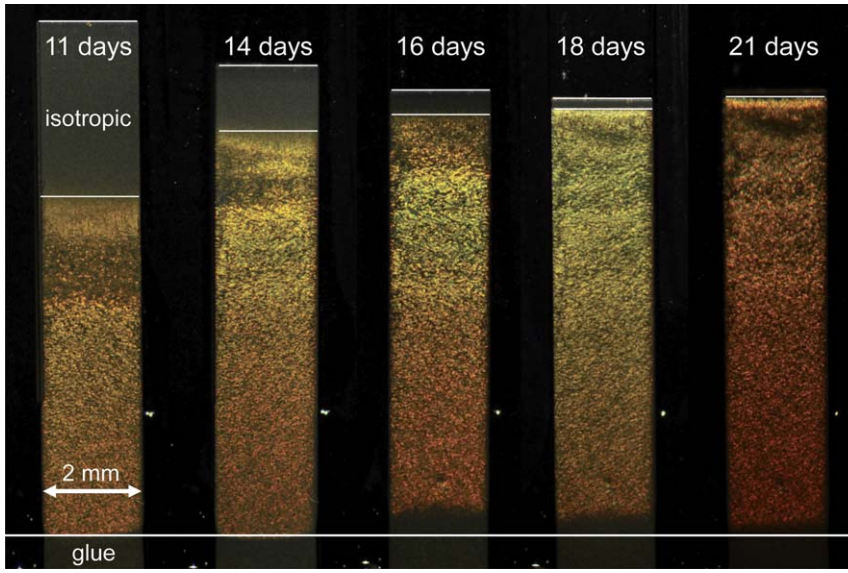

Fig. 2 A sedimenting sample of $L = 1.9$ μm, $D = 420$ nm rods followed in time. Photographs were taken while illuminating the sample from behind with white light. After several days, a Bragg-reflecting ordered region began to form in the bottom of the sample. In time, this region grew, while the interface between suspension and supernatant came down, indicating that rods are still sedimenting. After about 20 days the ordered region almost touched the interface, which stayed stable for the next weeks.

days of sedimentation. The formation of this ordered phase was initially faster than the sedimentation velocity (0.36 compared to 0.20 μm min^{-1} from day 11 to 14). The following days this region grew until it filled almost the whole sediment (after 21 days). Note that the density of Bragg reflecting areas in this phase changed in time; the top part of the Bragg reflecting area after 11 days showed less reflections than the same part of the sample after 14 days. The formation of ordered regions thus continued for several days.

The origin of the Bragg reflections was found using confocal microscopy (Fig. 3). In the area of little Bragg reflecting spots, small layered domains were found with dimensions of 20 to 50 μm in diameter and around 5 layers deep. Towards the bottom, where we can see more and stronger Bragg reflections, these areas increased to hundreds of microns and around 20 layers deep. The Bragg reflections thus result from the layered structures inside the sample. The fact that these do not span the whole capillary is due to the increasing concentration and multiple domains. Sedimentation is so fast that rotational and translational diffusion that facilitate ordering are hindered by the increasing density of the sample.

3.1 Sediments of rods studied by SAXS and CLSM

The phases in sediments of rod-like colloids with aspect ratios ranging from 3.7 to 8.0 were studied in more detail by SAXS and CLSM. Based on computer simulations for the HSC-system, a smectic liquid crystalline phase is expected for rods with an aspect ratio higher than 4.1, and a nematic phase for aspect ratios higher than 4.7.[33]

The sediment of the system with the largest aspect ratio ($L/D = 8.0$) shows, from top to bottom, an isotropic phase of about 0.5 mm high, followed by 3 mm of nematic phase and a smectic phase in the bottom 11 mm. SAXS patterns of these phases are shown in Fig. 4a–c. The scattering pattern of the isotropic phase shows

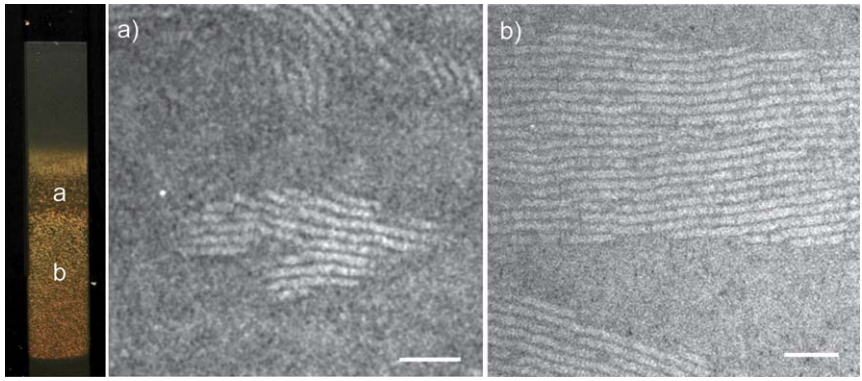

Fig. 3 Confocal microscopy images taken in the Bragg reflecting areas shown in Fig. 2. (a) Top part of the sediment with small layered domains. (b) Bottom part of the sediment with large layered domains. Scale bars indicate 10 μm.

weak signs of preferred orientation. This is caused by the size of the beam (around 0.3 mm), which is roughly equal to the height of the isotropic phase. Therefore, part of the nematic phase was also hit while imaging the isotropic phase. For the nematic phase, the intensity profile of the SAXS pattern shows a characteristic butterfly pattern with one broad peak that corresponds to the liquid-like ordering of neighboring rods (Fig. 4e), while no correlations were found in the length direction of the rods, corresponding to the literature.[34] Intensity profiles of the SAXS patterns of the smectic phase show very sharp peaks, up to the sixth order, due to diffraction from the layers of this phase that have a spacing of 2.4 μm. One broad peak at higher q-range originates from the liquid-like ordering of the rods within the layers

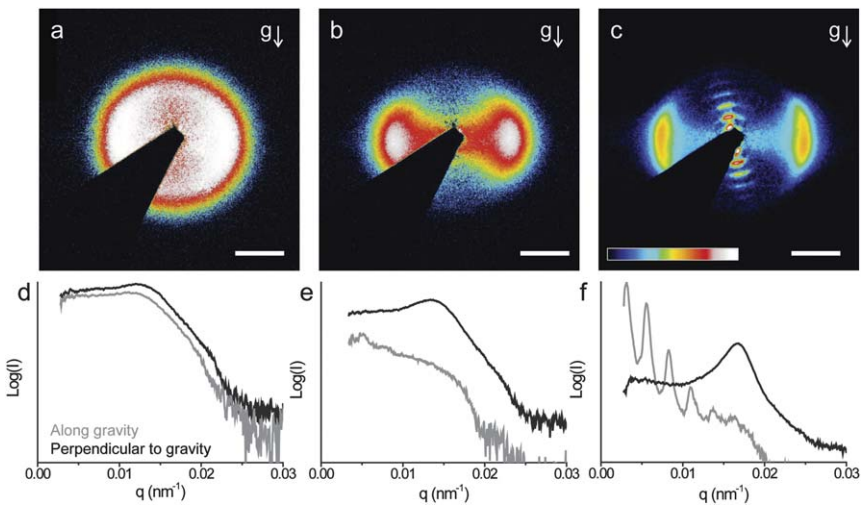

Fig. 4 SAXS measurements of a sediment of $L/D = 8.0$ rods. (a) Scattering pattern of the isotropic phase on a log-scale at a height of 14 mm from the bottom of the sample. (b) Scattering pattern of the nematic phase at a height of 12 mm. (c) Scattering pattern of the smectic-*C* phase at a height of 9 mm. (d–f) Intensity profiles of the patterns shown in (a–c) in the horizontal (black) and vertical (grey) direction, resp. perpendicular and along gravity *g*. Scale bars in (a), (b) and (c) indicate 0.01 nm^{-1}. The colored bar shows the false color - log-(intensity) scale with white color corresponding to the highest intensity.

(Fig. 4f). In this sample, the peaks originating from correlations in length are not oriented exactly perpendicularly to the peaks originating from correlations in diameter. This implies that the system formed a smectic-*C* phase, in which the rods within the layers are oriented at an angle of about 12° with respect to the layer's normal. This is probably caused by gravitational compression. Since the $L/D = 8.0$ rods were not fluorescently labeled, there are no real-space confocal microscopy images of this system available.

For slightly shorter rods ($L/D = 6.0$), all three liquid crystal phases were found as well (Fig. 5), but in this case also a phase that showed order within the layers was observed. In the bottom 11 mm of this sample a layered phase was found that shows stronger correlations within the smectic layers than the rods of $L/D = 8.0$. Three peaks were found at relative distances of 1, 1.8 and 2.8 ($q = 0.0098$, 0.0175 and 0.0274 nm^{-1}). These peaks suggest hexagonal ordering of the rods within the layers. For a perfect 2D hexagonal lattice, peaks are expected at relative distances of 1, $\sqrt{3}$, $\sqrt{4}$, $\sqrt{7}$ and $\sqrt{9}$. An explanation for the experimentally found distances is offered by the merging of the $\sqrt{3}$-peak and the $\sqrt{4}$-peak due to broadening, as well as the $\sqrt{7}$ and $\sqrt{9}$-peak. Hexagonal scattering patterns from such a structure were observed in a study on *fd*-virus as well.[35] The merging of the peaks is probably caused by the polydispersity of the sample, causing small variations in inter-particle distances. Because of its long-range hexagonal order within layers, but absence of crystalline correlations between layers, we identify this phase as a smectic-*B* phase.

On top of the smectic-*B* phase, a 3 mm high smectic-*A* phase was found (Fig. 5c,g,l). In the smectic-*A* phase there is no long-range positional order of rods within the layers. The peaks in the intensity profile of this phase are broader than those of the phase below, representing the more liquid-like ordering of this phase. The peaks that result from periodicity along the length of the rods, although present, are less well defined than those in the sample of longer rods. This corresponds well to the real-space measurements of this sample, depicted in Fig. 5l, which indicate that the layers show rather large fluctuations.

Higher up in the sample, a 1 mm high nematic phase was found (Fig. 5b,f,k). This phase also shows more correlations than the nematic phase of the longer rods: two peaks were found that correspond to correlations in the plane perpendicular to the nematic director. These peaks are related to presmectic ordering, which was also observed in computer simulations.[29] Compared to the layered phases of this sample, the peaks are broader, which indicates liquid-like order with more variations in inter-particle distances. The real-space confocal microscopy image of the nematic phase (Fig. 5k) shows the origin of the second peak: the rods showed a beginning of ordering into layers. Peaks that are caused by periodicities along the length of the rods are absent, which distinguishes a nematic from a smectic phase.

In the about 0.5 mm high isotropic phase that was found above the nematic all liquid crystalline order disappeared, represented by the isotropic scattering and the broad peaks of Fig. 5a and e. Very weak correlations are still present, as indicated by the small second order peak, but these cannot be found in the real-space image (Fig. 5j).

The more monodisperse system with $L/D = 5.0$ shows even stronger signs of hexagonal ordering (Fig. 6). The scattering pattern of this phase shows strong, sharp peaks for correlations within the layers that are spaced at relative distances of 1 (for the first peak), $\sqrt{3}$, $\sqrt{4}$ and $\sqrt{7}$ ($q = 0.0098$, 0.0169, 0.0195 and 0.0262 nm^{-1}), which indicates that the rods are hexagonally ordered within the layers. This is confirmed by confocal microscopy images of the phase. Fig. 7 shows the hexagonal layers from the top and two sides. Due to the lower resolution of the confocal microscope in the *z*-direction, the rods appear stretched in this direction. The hexagonal order within the layers is clearly visible in Fig. 7a. A cut through the *xy*-plane shows disorder in the stacking of the layers themselves, which is expressed in broad and small peaks in the SAXS pattern originating from correlations along the length. Although these observations hint towards a crystalline phase, no peaks due to correlations between

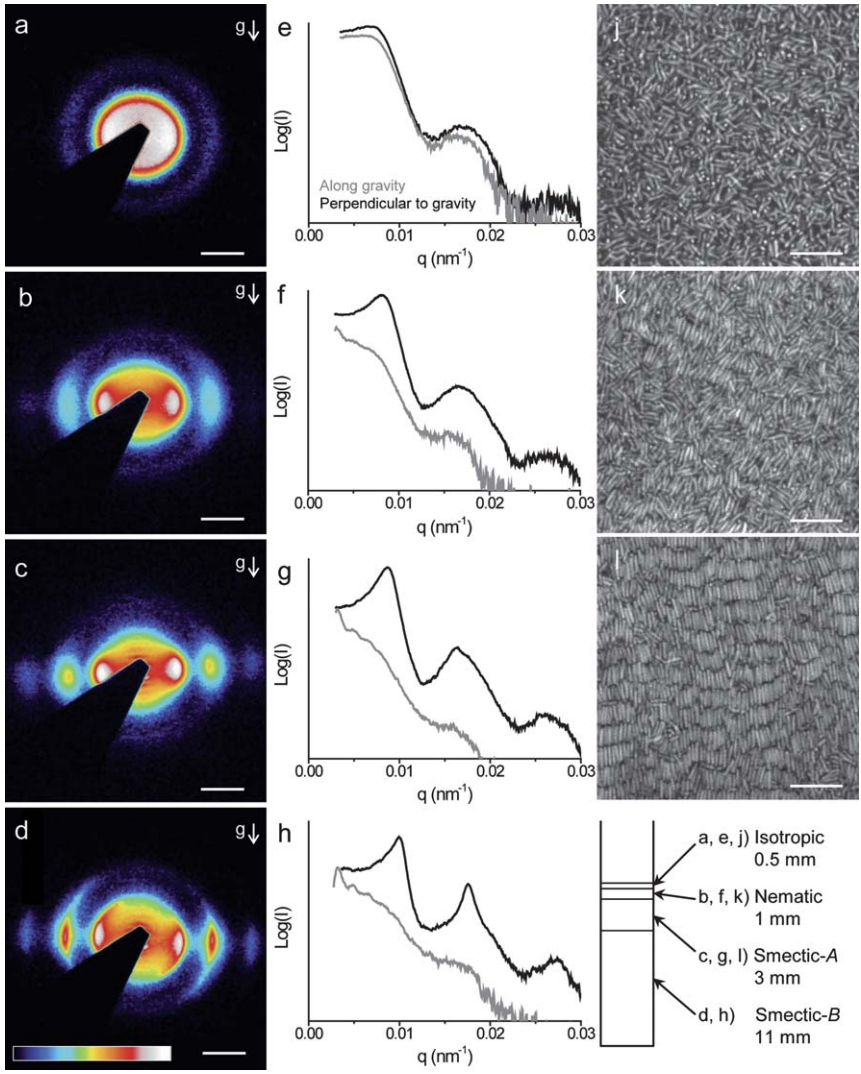

Fig. 5 SAXS measurements of a sediment of $L/D = 6.0$ rods. (a–d) SAXS patterns on a log-scale of the isotropic, nematic, smectic-*A* and smectic-*B* phase, respectively. Scale bars are 0.01 nm^{-1}. (e–h) Intensity profiles of the patterns shown in (a–d) in the horizontal (black) and vertical direction (grey). (j–l) Confocal microscopy images of the isotropic, nematic and smectic phase of the same sample. Scale bars indicate 10 μm. The colored bar shows the false color - log(intensity) scale with white color corresponding to the highest intensity.

the hexagonal patterns of subsequent layers were found, which excludes the structure being fully crystalline in three dimensions. Therefore, we identified the structure as a smectic-*B* phase. Higher up in this sample we found a smectic-*A*, a nematic and finally an isotropic phase.

For the system of rods with the shortest aspect ratio ($L/D = 3.7$), hexagonally ordered rods were found in domains that extended tens of microns, as shown in Fig. 8a. The degree of hexagonal order in these layers is shown in Fig. 8b, which shows the 2D radial distribution function of the rods as compared to that of a perfect 2D hexagonal lattice. The experimental peaks were scaled to fit the first peak of the theoretical $g(r)$ and extend over 10 particle diameters, comparing well

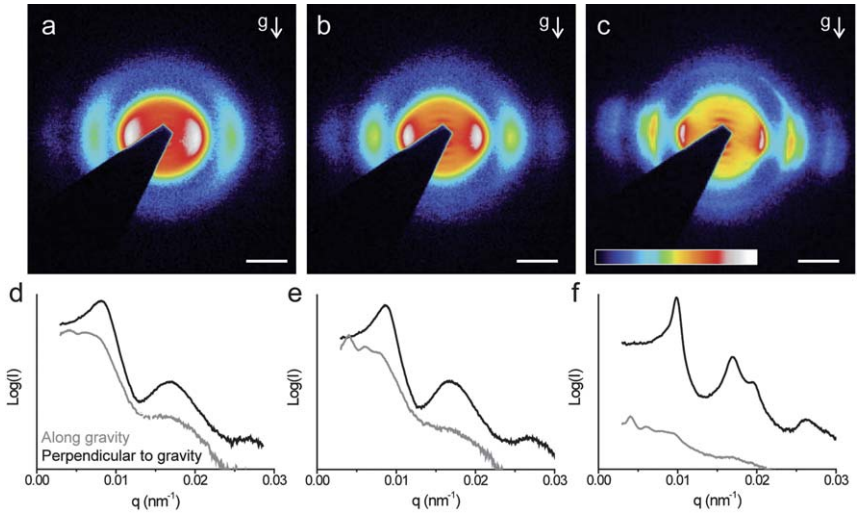

Fig. 6 SAXS measurements of $L/D = 5.0$ rods. (a–c) Scattering patterns of the nematic, smectic-A and smectic-B phase, respectively. (d–f) Intensity profiles of the patterns shown above in the horizontal (black) and vertical direction (grey). Scale bars indicate 0.01 nm^{-1}. The colored bar shows the false color - log(intensity) scale with white color corresponding to the highest intensity.

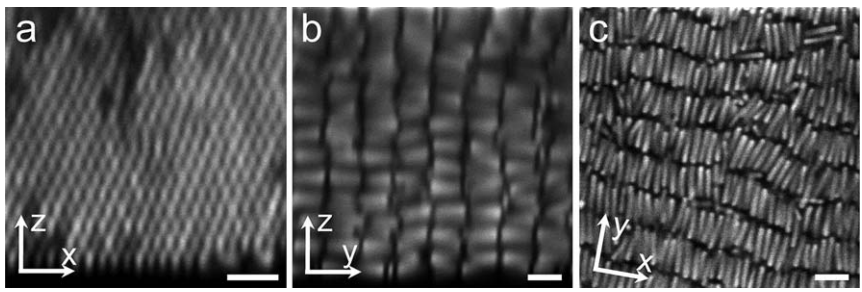

Fig. 7 Confocal microscopy images of hexagonally ordered layers in a sediment of $L/D = 5.0$ rods through different planes. Scale bars indicate 3 μm.

to the $g(r)$ of the perfect lattice. The average distance between the centers of the rods was 910 nm, while the diameter measured by TEM was 640 nm. The difference is caused mostly by the negative charge on the silica rods, causing repulsive interactions, and partly by the fact that these measurements were not performed at the densest packing. The degree of hexagonal order in the sample was quantified by the 2D local hexagonal bond orientational order parameter ψ_6:[36]

$$\psi_6(r_j) = \frac{1}{N}\sum_k \exp\left(i6\theta(r_{jk})\right) \quad (1)$$

where k runs over all N neighboring particles (determined by Delaunay triangulation) of particle j and $\theta(r_{jk})$ is the angle between the vector between particles j and k and a fixed reference axis. The value of $|\psi_6|$, which is a number between 0 (no order) and 1 (perfectly crystalline), gives the degree of hexagonal order around each particle, $\langle\psi_6\rangle$ denotes this value as averaged over all particles. In the crystalline sheets found in sediments of short rods, $\langle\psi_6\rangle$ was around 0.75. Confocal images of larger areas are needed to determine whether the ordering in these samples is

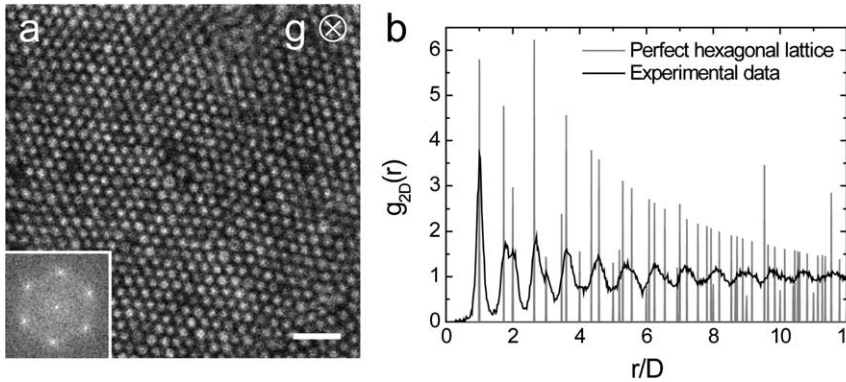

Fig. 8 (a) Confocal microscopy image of short rods (L $D^{-1} = 3.7$) sedimented in a flat capillary. Large areas of hexagonally ordered rods are visible. In the inset a Fourier transform of the image is shown. Scale bar indicates 5 μm. (b) 2D Radial distribution function of a hexagonally ordered sheet of rods in black. The equivalent for a perfect hexagonal lattice is shown in grey.

really hexagonal or hexatic. Fig. 8a further shows the Fourier transform of the confocal image, in which the first six peaks corresponding to hexagonal ordering are visible. This image corresponds well to the SAXS patterns of the sample, which shows six peaks spaced at approximately 60° up to two scattering orders (Fig. 9a). Although in most of the sample the layers were oriented with rods parallel to the wall of the capillary (Fig. 9c,d), we were able to find some domains with the rods perpendicular to the wall, as in Fig. 9a,b. The crystalline phase continued higher up in the sample until the scattering pattern of an isotropic phase was seen. Smectic-*A* or nematic phases were not observed in the $L/D = 3.7$ sample.

3.2 Phase diagram

The measurements described in the previous section can be summarized in a rough phase diagram (Fig. 10). To estimate the volume fractions of the phases observed, inter-particle distances L_s and D_s were determined at different heights in the capillary from the SAXS measurements. Subsequently, the volume fractions of the different phases were calculated as follows. In the smectic-*B* phase, the volume fraction was calculated by dividing the volume of the rods that was measured by TEM (assuming the shape of a cylinder with one hemispherical cap) by the available volume per particle measured by SAXS: $\frac{1}{2}\sqrt{3}D_s^2L_s$. For a smectic-*A* phase there is no hexagonal order between the rods and the available volume per particle was estimated by $D_s^2L_s$. In case of a nematic, the extra distance along the length of the rods was assumed to be equal to the calculated difference for the diameter. In order to compare the experimental data with computer simulations, the volume fractions were normalized with respect to the volume fraction at close packing φ_{cp}. Since there were no correlations found between neighboring layers, we assume $\varphi_{cp} = \frac{\pi}{2\sqrt{3}}\left(1 - \frac{D}{6L}\right)$ (hexagonally close-packed rods in one layer). The resulting experimental phase diagram is shown in Fig. 10a.

Our experimental results show many similarities with the phase diagram computed by Bolhuis and Frenkel.[33] Isotropic phases were found at low volume fractions, and for higher volume fractions, nematic and smectic phases were found. At the highest volume fractions, however, Bolhuis and Frenkel found a crystalline phase, while we identified our phase as a smectic-*B* phase. These phases are actually very much alike. The difference between the two is the presence (for the crystal) or

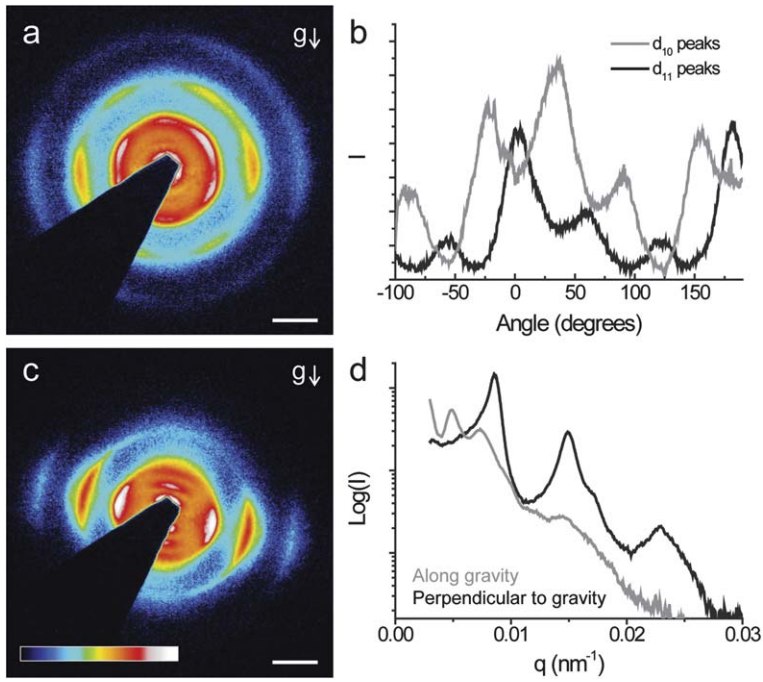

Fig. 9 SAXS pattern of hexagonally ordered rods ($L/D = 3.7$) in two orientations. (a) Rods perpendicular to the capillary wall. (b) Intensity profile of the hexagonal peaks integrated over the circles shown in (a). (c) Rods parallel to the capillary wall. (d) Intensity profiles of the pattern shown in (b). Scale bars indicate 0.01 nm^{-1}. The colored bar shows the false color - log(intensity) scale with white color corresponding to the highest intensity.

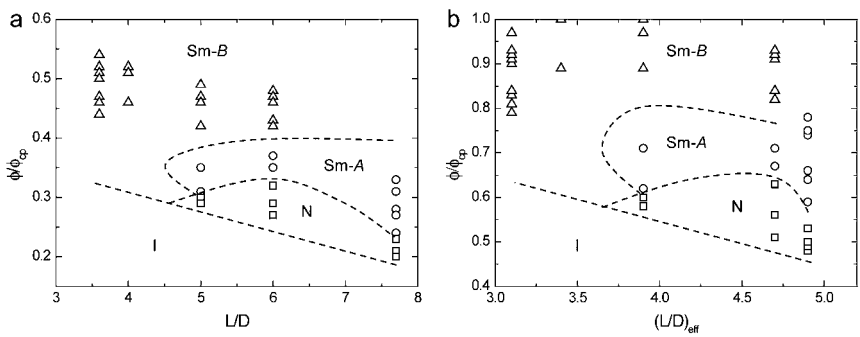

Fig. 10 (a) Experimental phase diagram for silica rods depending on aspect ratio and density. The volume fractions of the smectic-*B* phase are depicted as triangles, circles denote the smectic-*A* phase and squares the nematic phase. Lines were drawn as a guide to the eye. (b) Phase diagram corrected for electric double layer repulsions by taking an effective hard-rod diameter and length.

absence (for the smectic-*B*) of correlations between subsequent layers.[37] Since we did not find proof of correlations between the layers, we refer to the structure as smectic-*B*. The formation of a smectic-*B* instead of a full crystalline phase is probably caused by the polydispersity of the systems used (around 10%). Also, charge may play a role. According to simulations, the layer spacing is less than 1.048 times the length of the rods for aspect ratios from 3 to 5 in the smectic phase.[38] In our systems, the

layer spacing was often larger (on the order of 1.1 to 1.2 times L_{eff}), which may be the reason that the layers were not correlated.

Also similar to the simulations, the isotropic-nematic phase boundary of the experimental phase diagram shows the same dependence on the aspect ratio: the volume fraction at which the transition occurs decreases with increasing aspect ratio. Furthermore, smectic and nematic phases were found only at aspect ratios of 5 and higher, which is in correspondence with the simulations that predicted nematics for $L/D > 4.7$ and smectics for $L/D > 4.1$.

A large discrepancy between experiments and simulations was found, as fully expected, in the volume fraction of the phases. The experimentally determined volume fractions are significantly lower than those calculated by computer simulations. This is caused by the fact that the experimental system is not a perfect hard rod system. The silica particles are negatively charged and therefore experience repulsive interactions. In literature, it was shown for virus suspensions that the isotropic-nematic volume fractions are described well by an increased effective diameter.[39] The nematic-smectic volume fractions rescaled in this way disagreed with the hard rod model, however, except at high ionic strength.[40] Since in our case the double layer thickness is much smaller than the rod diameter a rescaling should be acceptable. The effective diameter D_{eff} was determined by measuring the minimum inter-particle distances between the rods at the bottom of the sediment, where we assume the rods to be close packed. The effective length was assumed to be $L + D_{eff} - D$, where L and D are the hard-rod dimensions, measured by TEM. The hard-rod and effective dimensions are listed in Table 2 and the rescaled phase diagram is shown in Fig. 10b. For this "effective hard-rod" phase diagram, the volume fractions correspond well with the simulations, but the effective aspect ratio's do not. Nematic and smectic phases occur now for aspect ratios of 3.9 and higher. Apparently, this method of correcting for the double layer, that worked well for spheres, does not map our results onto the HSC phase diagram exactly.

In literature, several other examples of short rods forming smectic phases exist. Maeda *et al.*, for example, observed isotropic-smectic transitions for selenium and β-FeOOH rods of $L/D = 3.5$–8.0.[11,41] Their observations for these low aspect ratios correspond well with our observations, including hexagonal ordering of the rods with $L/D = 3.5$ and side-by-side ordering in clusters before forming a smectic(-*B*) phase. Nematic phases, however, were only observed for $L/D = 10$–35 in this study. Maeda *et al.* did not correct for repulsions or polydispersity in their work, which they claim could be the cause of the difference with the simulations, which predicted nematics from $L/D = 4.7$. In our experience, the nematic phase was hard to find by real-space measurements, because it occurs only in a small range of densities. Guided by the SAXS-measurements and having the ability to image 2D slices in dense sediments by confocal microscopy, we were able to find a thin layer of rods in a nematic phase (Fig. 5k) where they might have been missed by Maeda *et al.*, who used a standard optical microscope.

Table 2 Hard rod dimensions as measured by TEM and effective rod dimensions as measured by SAXS. Here, L is the length of the rods, D the diameter, and L/D the aspect ratio

	Hard rod dimensions			Effective rod dimensions		
	L/μm	D/nm	L/D	L_{eff}/μm	D_{eff}/nm	$(L/D)_{eff}$
B31	2.37	640	3.7	2.56	830	3.1
B35	3.3	550	6.0	3.49	740	4.7
B36	1.9	235	8.0	2.1	430	4.9
B48	2.6	630	4.1	2.8	830	3.4
N51	2.66	530	5.0	2.86	730	3.9

Other well known liquid crystal systems that show nematic phases, such as TMV or *fd*-virus all have larger aspect ratios than the rods studied in this chapter ($L/D <$ 8).[5,39,40] Also for boehmite rods, nematic phases were only observed for larger aspect ratios.[42] For goethite particles, nematic phases were observed for $L/D = 3.5$, but these particles are much thinner in the third dimension ($L/T \sim 10$, with T as their thickness).[43]

3.3 Influence of the flat wall

In experimental studies of colloidal dispersions, boundary effects (such as the flat wall of the cell that contains the dispersion) are always present. For spheres, it was found that the presence of a flat wall can lead to layering and eventually pre-freezing of a liquid phase.[44,45] Also, the effect of a flat wall on crystallization has been studied intensively.[23,46] The effect of a flat wall on the ordering of rods was examined using computer simulations.[47,48] Here, it was found that a thick nematic film forms on the wall in the isotropic phase.

For our system of hard rods, we experimentally confirmed that the rods tend to align with their long axis parallel to the flat surface. In capillaries positioned with their flat wall to the bottom, we found that the rods always lay flat on the bottom. This resulted in layered phases that were always oriented with their layers perpendicular to the bottom plane. In standing capillaries, for which the flat wall was positioned in the vertical direction, the rods were found to orient again parallel to the flat wall, pointing down this time. This orientation was found in both the confocal and the scattering data, *e.g.* in Fig. 5. Additionally, we found that the influence of the wall extended tens of microns into the sample, after which domains of random orientations of the formed phase were observed.

3.4 Nucleation and defects in smectic phases

Although we did not specifically investigate the phenomenon of the nucleation of crystal or liquid crystal phases, we can indirectly infer some conclusions with respect to the nucleation of the smectic phase as can be seen in Fig. 11a and b. In Fig. 11a a smectic-*B* phase consisting of just a few layers can be seen below an isotropic phase in a sedimenting system of rods with an aspect ratio of 3.7. Fig. 11b shows that adjacent planes tended to stack perpendicularly. Ni *et al.* described the crystal nucleation of a system of hard rods with an aspect ratio of 3 using computer simulations.[49] At lower supersaturation, the nucleation of multilayered crystalline structures was observed much like those visible in Fig. 11a/b (compare with Fig. 11c). At higher supersaturation, small randomly oriented small crystallites were observed that got kinetically trapped (Fig. 11d). The cubatic order of these crystallites corresponds well with the experimentally observed perpendicular orientation of domains like those in Fig. 11b.

The agreement with the computer simulations, which try to identify the equilibrium path, and our preliminary experimental results on the nucleation of the smectic and/or crystal phases of the rods is quite satisfactory. However, it is also a recent finding of our group, based on experiments on hard sphere-like particles, that even for crystal nucleation and growth that is done relatively slowly as to stay close to equilibrium, the system does not follow equilibrium growth with respect to *e.g.* the number of defects quite quickly after the nucleation phase.[50] Also, these experiments and findings on growing 3D crystals on preformed 2D nuclei arranged by optical tweezers were supported by computer simulations. According to us, a clear way on how these non-equilibrium aspects can be adequately incorporated in a theory, or, related to this, how can be judged how far away from equilibrium the crystal nucleation and growth takes place in experiments, are still important open questions. Perhaps colloidal model systems are a way in which these questions can

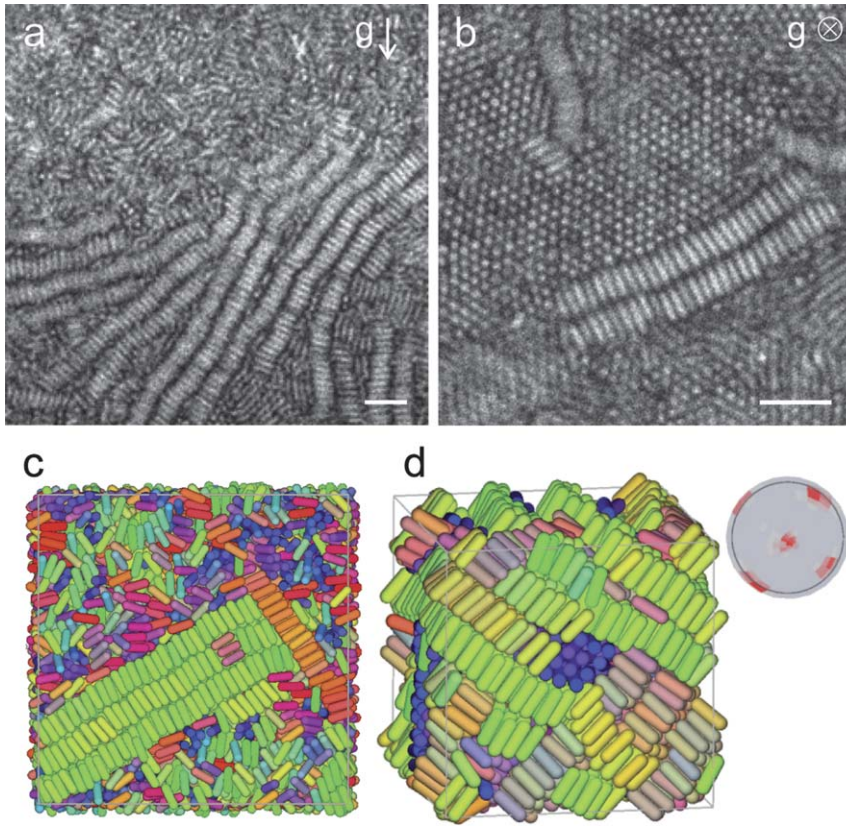

Fig. 11 Nucleation of short rods. (a) Confocal microscopy image of rods with an aspect ratio of 3.7. An isotropic phase is visible in the top of the image, with a smectic-*B* phase below. (b) Image inside a smectic-*B* plane, showing the perpendicular stacking of the domains. Scale bars indicate 5 μm. (c) Simulation result at a pressure $p^* = 7.6$. A smectic nucleus is formed in the isotropic phase. The different colors denote the different orientations of the rods. (d) Simulation result at a pressure $p^* = 8$. The system ends up in a jammed state with cubatic order. The angular distribution of the particles' orientation is shown in the unit sphere beside the configuration. The simulation images c and d were provided by the authors of ref. 49.

also be addressed for atomic and molecular systems, even though the dynamics in the two systems are different.

The appearance of the smectic phases found varied strongly as a function of the aspect ratio of the rods. For long aspect ratios (>6), layer formation occurred more readily and large domains formed that extended over the whole sample. Defects that were found in these samples include mainly edge dislocations and splay distortions (Fig. 12a). In samples of shorter rods, defects were observed more frequently. Also, the domains found in these samples were smaller than for long rods. Fig. 12b shows three types of defects. The first type, inside circle 1, is that neighboring domains or defect layers are positioned perpendicularly with respect to each other. Inside circle 2 the ending of a layer is shown, called an edge dislocation. Both types of defects have been described for other liquid crystal systems.[51] The third type of defect, however, has not been observed before experimentally as far as we know. This defect, which is called a transverse interlayer (TI) particle, is described as a rod positioned in between the layers of a smectic and oriented with its long axis parallel to the layers. TI particles have a higher free energy than particles inside the layers. Since the presence of TI particles minimizes the free energy of the

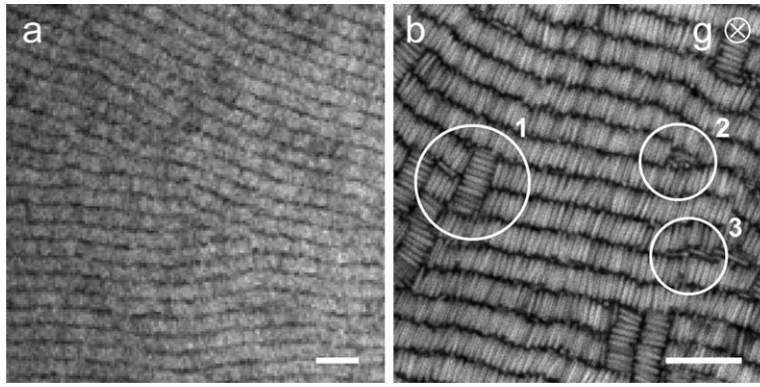

Fig. 12 Confocal microscopy images showing several types of defects. (a) Edge dislocations and splay distortions in a sample with rods of aspect ratio 8.7. (b) Sediment of $L/D = 6$ rods. 1) Small domain oriented perpendicular to its neighbor-domains. 2) Edge dislocation. 3) Transverse-interlayer (TI) particles. Scale bars indicate 10 μm.

configuration, this type of defects cannot be annealed out. The existence of TI particles was predicted by computer simulations already in 1995,[52,53] but no experimental confirmation of the phenomenon has been reported up to now. In the simulations it was found that the abundance of TI-particles depends on the smectic layer spacing λ. The simulations were done for $\lambda = 1.03$, while in our experiments $\lambda \sim 1.13$. This might explain why we found more TI particles than expected; we found on the order of a few percent of the rods to be TI particles, while the simulations resulted in a fraction on the order of 10^{-5}.

3.5 Dynamics in the smectic phase

Beside the previously described structural aspects of the different liquid crystal phases, there are also dynamical differences. The diffusion of rods in liquid crystalline phases was found to be greatly affected by the increased structural order. Computer simulations and experiments showed that in nematic phases the long-time self-diffusion coefficient along the director $D_{\parallel}$ is higher than the one perpendicular to the director $D_{\perp}$.[54] A ratio of $D_{\parallel}/D_{\perp} = 2$ to 4 was found near the isotropic-nematic transition, which increased with increasing concentration. In a smectic, however, $D_{\parallel}$ is expected to decrease dramatically, to even below $D_{\perp}$. Below, we describe some preliminary observations on dynamics in one of our smectic phases.

A dynamic difference between the smectic and the crystalline phase is that long-time self-diffusion only occurs in smectics and not in crystals. To determine whether the layered phase formed by rods with a length of 1.4 μm and a diameter of 280 nm is a smectic, we studied the diffusion of the rods mostly qualitatively. Due to their small diameter, single particle imaging of these rods was not possible, but the layers of the structure are clearly visible in Fig. 13. A 50×50 μm^2 x-z plane was bleached perpendicular to the orientation of the layers by scanning this plane 10 times in short succession (Fig. 13 top row). In time, the bleached particles diffused to the non-bleached area and *vice versa*, resulting in a spread of the dark area in the images. Since there is clearly diffusion of rods, the layered phase is indeed a smectic. When a plane parallel to the layers (in other words: one of the layers) was bleached, the spreading was slower and the boundary between the bleached and non-bleached area stayed much sharper. These observations confirm the simulation results on hard spherocylinders by Löwen, who found that $D_{\perp} > D_{\parallel}$ in smectics.[54] Intuitively, this is easy to understand since the rods are ordered liquid-like inside the layers and diffusion is therefore easy. In the direction perpendicular to the layers the structure is

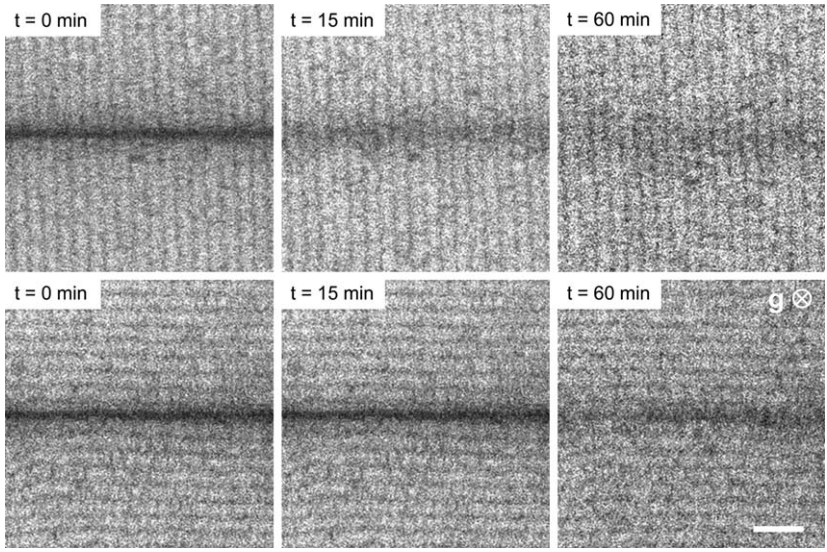

Fig. 13 Diffusion of bleached particles with aspect ratio 5.0 within smectic planes (upper row) and from plane to plane (lower row). Scale bar indicates 5 μm.

ordered, which makes diffusion slower because an energy barrier has to be overcome. However, exactly the opposite was found in diffusion studies on the *fd*-virus, where self-diffusion takes place preferentially in the direction perpendicular to the smectic layers and occurs by quasiquantized steps of one rod length.[55,56] This is possibly caused by the flexibility of the virus particles. In a rough estimation from Fig. 13 we found $D_{\perp} \sim 0.2\ \mu m^2\ s^{-1}$ in our system.

Diffusion on the single particle level for thin rods was studied using a mixture of labeled and unlabeled rods, similarly as was done for *fd*-virus.[6] The labeled rods were thicker than the unlabeled rods in this case (340 *versus* 250 nm). Sedimentation of a sample with a 1 : 100 ratio of labeled : unlabeled rods and an initial volume fraction of 0.17 resulted in the formation of a smectic phase. In this tracer system, it is possible to observe single particles with small diameters in the smectic phase.

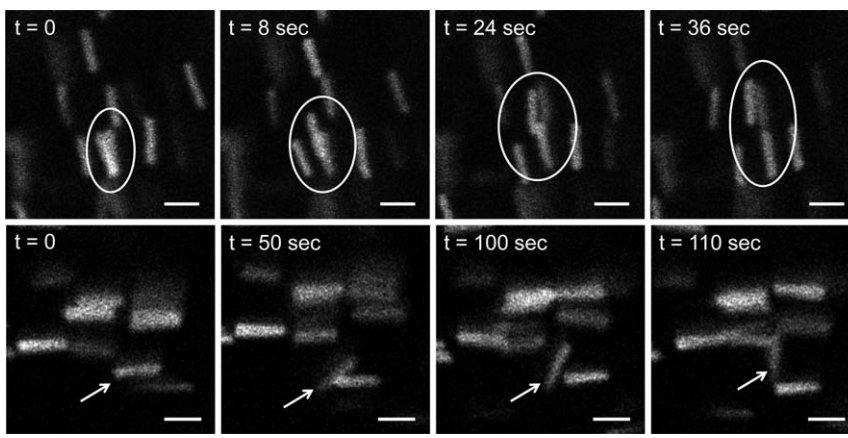

Fig. 14 On a single particle level: diffusion from one smectic plane to another (upper row) and formation of a transverse-interlayer particle (lower row). Scale bars indicate 2 μm.

From measurements just above the nematic/smectic transition we found $D_{\perp} \sim 0.5$ $\mu m^2\ s^{-1}$. Besides diffusion within the layers, we also found more rare events like hopping from one layer to another and the transformation from normal rod to TI-particle (Fig. 14). The single particle hopping from one layer to another or from in-layer to transverse-interlayer particles shows a striking resemblance with the particle trajectories as observed in computer simulations by Patti *et al.*[38] The hopping phenomenon was studied in more detail by computer simulations,[38,57,58] as well as experiments on *fd*-virus.[55]

4 Conclusions

The phase behavior of rod-like silica particles with aspect ratios smaller than 8 was determined using small angle X-ray scattering and confocal laser scanning microscopy. The results were summarized in a phase diagram, which corresponds well with computer simulations on HSC-systems. In correspondence with the simulations, no liquid crystalline phases were found for silica rods with small aspect ratios. Nematic and smectic phases were found for aspect ratios of 5.0 and higher, while simulations predict nematics for $L/D > 4.7$ and smectics for $L/D < 4.1$. Instead of forming a fully crystalline phase, the rods ordered into a hexagonally ordered smectic-*B* phase at high volume fractions, probably due to their length polydispersity ($\sim$10%) and/or their charge which causes larger layer spacings. The experimentally found volume fractions of the different phases were significantly lower than those calculated in the simulations, which is caused by the negative charge of the rods. The resulting electric double layer increased the effective dimensions of the rods and decreased the volume fraction.

The system of colloidal silica rods that was used in this work is unique because it allows us to examine liquid crystalline phases at the single particle level in 3D. Thus, we have not only studied the structure of fully developed liquid crystal phases with both scattering and microscopy, but also identified a number of different defect structures that we encountered. Though admittedly more preliminary, we found, using real space techniques, strong indications that confirmed the nucleation process for short rods that was found by computer simulations. Also, several types of defects in the smectic phase were found. The amount of defects decreased with increasing aspect ratio. Because the rods could be imaged on the single particle level, the existence of transverse interlayer particles was observed experimentally for the first time. Also, dynamical processes such as diffusion within and between layers as well as the transition from in-layer to transverse-interlayer particle were observed. The order of magnitude of the diffusion coefficient, determined by these preliminary measurements corresponds to measurements on other rod-like colloidal systems. We believe that our rod-like silica colloids form an excellent system to study these properties of liquid crystalline suspensions in more detail.

Acknowledgements

We would like to thank Bart de Nijs for his help with the SAXS measurements. The staff of the BM26 beamline of the ESRF is acknowledged for their excellent support. NWO is acknowledged for the beam time. Furthermore, we thank Ran Ni for providing the simulation images and Marjolein Dijkstra for critical reading of the manuscript. This work was funded by the High Potential Program of Utrecht University and by the EU (NANODIRECT, grant number CP-FP 213948-2).

References

1 L. Onsager, *Ann. N. Y. Acad. Sci.*, 1949, **51**, 627–659.
2 D. Frenkel and B. M. Mulder, *Mol. Phys.*, 1985, **55**, 1171.
3 D. Frenkel, H. N. W. Lekkerkerker and A. Stroobants, *Nature*, 1988, **332**, 822–823.

4 G. J. Vroege and H. N. W. Lekkerkerker, *Rep. Prog. Phys.*, 1992, **55**, 1241–1309.
5 Z. Dogic and S. Fraden, *Curr. Opin. Colloid Interface Sci.*, 2006, **11**, 47–55.
6 M. P. Lettinga, E. Barry and Z. Dogic, *Europhys. Lett.*, 2005, **71**, 692–698.
7 B. J. Lemaire, P. Davidson, J. Ferré, J. P. Jamet, D. Peterman, P. Panine, I. Dozov and J. P. Jolivet, *Eur. Phys. J. E*, 2004, **13**, 291–308.
8 B. J. Lemaire, P. Davidson, J. Ferré, J. P. Jamet, D. Peterman, P. Panine, I. Dozov and J. P. Jolivet, *Eur. Phys. J. E*, 2004, **13**, 309–319.
9 E. van den Pol, A. V. Petukhov, D. M. E. Thies-Weessie, D. V. Byelov and G. J. Vroege, *J. Colloid Interface Sci.*, 2010, **352**, 354–358.
10 E. van den Pol, A. A. Verhoeff, A. Lupascu, M. A. Diaconeasa, P. Davidson, I. Dozov, B. W. M. Kuipers, D. M. E. Thies-Weesie and G. J. Vroege, *J. Phys.: Condens. Matter*, 2011, **23**, 194108.
11 H. Maeda and Y. Maeda, *Phys. Rev. Lett.*, 2003, **90**, 018303.
12 K. M. Keville, E. I. Franses and J. M. Caruthers, *J. Colloid Interface Sci.*, 1991, **144**, 103.
13 C. C. Ho, A. Keller, J. A. Odell and R. H. Ottewill, Colloid Polym, *Sci.*, 1993, **271**, 469.
14 A. F. Demirörs, P. M. Johnson, C. M. van Kats, A. van Blaaderen and A. Imhof, *Langmuir*, 2010, **26**, 14466–14471.
15 C. M. van Kats, P. M. Johnson, J. E. A. M. Meerakker and A. van Blaaderen, *Langmuir*, 2004, **20**, 11201–11207.
16 A. Kuijk, A. van Blaaderen and A. Imhof, *J. Am. Chem. Soc.*, 2011, **133**, 2346–2349.
17 A. Vrij, J. W. Jansen, J. K. G. Dhont, C. Pathmamanoharan, M. M. Kops-Werkhoven and H. M. Fijnaut, *Faraday Discuss. Chem. Soc.*, 1983, **76**, 19–35.
18 A. van Blaaderen and P. Wiltzius, *Science*, 1995, **270**, 1177–1179.
19 A. Kuijk, A. Imhof and A. van Blaaderen, *Langmuir*, 2012, submitted.
20 M. A. Bates and D. Frenkel, *J. Chem. Phys.*, 1998, **109**, 6193–6199.
21 A. Stroobants, H. N. W. Lekkerkerker and T. Odijk, *Macromolecules*, 1986, **19**, 2232.
22 E. Eggen, M. Dijkstra and R. van Roij, *Phys. Rev. E: Stat., Nonlinear, Soft Matter Phys.*, 2009, **79**, 041401.
23 J. P. Hoogenboom, P. Vergeer and A. van Blaaderen, *J. Chem. Phys.*, 2003, **119**, 3371–3383.
24 A. van Blaaderen, J. Peetermans, G. Maret and J. K. G. Dhont, *J. Chem. Phys.*, 1992, **96**, 4591–4603.
25 E. M. Kramer and J. Herzfeld, *Phys. Rev. E: Stat. Phys., Plasmas, Fluids, Relat. Interdiscip. Top.*, 2000, **61**, 6872–6878.
26 H. Graf and H. Löwen, *Phys. Rev. E: Stat. Phys., Plasmas, Fluids, Relat. Interdiscip. Top.*, 1999, **59**, 1932.
27 J. C. Crocker and D. G. Grier, *J. Colloid Interface Sci.*, 1996, **179**, 298.
28 A. V. Petukhov, J. H. H. Thijssen, D. C. 't Hart, A. Imhof, A. van Blaaderen, I. P. Dolbnya, A. Snigirev, A. Moussaid and I. Snigireva, *J. Appl. Crystallogr.*, 2006, **39**, 137–144.
29 S. V. Savenko and M. Dijkstra, *Phys. Rev. E: Stat., Nonlinear, Soft Matter Phys.*, 2004, **70**, 051401.
30 S. Boersma, *J. Chem. Phys.*, 1960, 32.
31 M. M. Tirado, C. L. Martinez and J. Garcia de la Torre, *J. Chem. Phys.*, 1984, **81**, 2047–2052.
32 Z. Dogic, A. P. Philipse, S. Fraden and J. K. G. Dhont, *J. Chem. Phys.*, 2000, **113**, 8368–8380.
33 P. G. Bolhuis and D. Frenkel, *J. Chem. Phys.*, 1997, **106**, 666.
34 K. R. Purdy, Z. Dogic, S. Fraden, A. Rühm, L. Lurio and S. G. J. Mochrie, *Phys. Rev. E: Stat. Phys., Plasmas, Fluids, Relat. Interdiscip. Top.*, 2003, **67**, 031708.
35 E. Grelet, *Phys. Rev. Lett.*, 2008, **100**, 168301.
36 C. Murray, Experimental studies of melting and hexatic order in two-dimensional colloidal suspensions, in: *Bond-orientational order in condensed matter systems*, Springer-Verlag, New York, 1992, pp. 137–215.
37 P. G. de Gennes and J. Prost, *The physics of Liquid Crystals*, Oxford University Press, 2nd edn, 1995.
38 A. Patti, D. El Masri, R. van Roij and M. Dijkstra, *J. Chem. Phys.*, 2010, **132**, 224907.
39 K. R. Purdy and S. Fraden, *Phys. Rev. E: Stat., Nonlinear, Soft Matter Phys.*, 2004, **70**, 061703.
40 K. R. Purdy and S. Fraden, *Phys. Rev. E: Stat., Nonlinear, Soft Matter Phys.*, 2007, **76**, 011705.
41 H. Maeda and Y. Maeda, *J. Chem. Phys.*, 2004, **121**, 12655.
42 P. A. Buining, A. P. Philipse and H. N. W. Lekkerkerker, *Langmuir*, 1994, **10**, 2106–2114.
43 E. van den Pol, D. M. E. Thies-Weesie, A. V. Petukhov, G. J. Vroege and K. Kvashnina, *J. Chem. Phys.*, 2008, **129**, 164715.
44 D. J. Courtemanche, T. A. Pasmore and F. van Swol, *Mol. Phys.*, 1993, **80**, 861–875.
45 M. Dijkstra, *Phys. Rev. Lett.*, 2004, **93**, 108303.

46 S. Dittrich, *Phase transitions and critical phenomena*, Academic Press, London, 1988.
47 M. Dijkstra, R. van Roij and R. Evans, *Phys. Rev. E*, 2001, **63**, 051703.
48 L. Harnau and S. Dietrich, *Phys. Rev. E*, 2002, **66**, 051702.
49 R. Ni, S. Belli, R. van Roij and M. Dijkstra, *Phys. Rev. Lett.*, 2010, **105**, 088302.
50 M. Hermes, E. C. M. Vermolen, M. E. Leunissen, D. L. Vossen, P. D. J. van Oostrum, M. Dijkstra and A. van Blaaderen, *Soft Matter*, 2011, **7**, 4623–4628.
51 Y. Iwashita and H. Tanaka, *Phys. Rev. E*, 2008, **77**, 041706.
52 R. van Roij, P. G. Bolhuis, B. Mulder and D. Frenkel, *Phys. Rev. E*, 1995, **52**, 1277–1281.
53 J. S. van Duijneveldt and M. P. Allen, *Mol. Phys.*, 1997, **90**, 243–250.
54 H. Löwen, *Phys. Rev. E*, 1999, **59**, 1989–1995.
55 E. Grelet, M. P. Lettinga, M. Bier, R. van Roij and P. van der Schoot, *J. Phys.: Condens. Matter*, 2008, **20**, 494213.
56 M. P. Lettinga and E. Grelet, *Phys. Rev. Lett.*, 2007, **99**, 197802.
57 R. Matena, M. Dijkstra and A. Patti, *Phys. Rev. E*, 2010, **81**, 021704.
58 A. Patti, D. El Masri, R. van Roij and M. Dijkstra, *Phys. Rev. Lett.*, 2009, **103**, 248304.